有機合成では技術の進歩により多くのオリゴ糖鎖を合成することが可能になってきている。糖鎖構造の多様性と分岐の存在により配列がひとつ長くなる毎にその合成技術は高度なものとなり、収率も急激に低下してしまう。そのような糖鎖合成の難しさを克服するためにone-potグリコシル化反応(1)や固相合成法(2)の開発は有効な手段となると期待されている。酵素合成では、加水分解酵素の逆反応や糖転移酵素を用いた糖鎖合成が行われている(3)。酵素を用いれば、有機合成に比較して簡単にオリゴ糖鎖を合成することが可能である。そのためには、まず多様な糖鎖構造を作り出せる酵素を準備する必要がある。300種類と言われている糖鎖合成酵素の遺伝子を解析するプロジェクトも進められており、一部の糖転移酵素は人工的に作ることも可能になってきている(4)。これに対して、筆者らは動物細胞を用いてオリゴ糖鎖を細胞工学的に作り出す方法を提案している。この方法では難しい有機合成の技術が不要であり、また糖鎖合成遺伝子のクローニング、および酵素や糖ドナーを準備する必要がない。

現在市販で入手できるオリゴ糖鎖は、種類が限られており、価格も高い。自分が必要とするオリゴ糖鎖をオーダーメイドで注文するシステムも十分には確立されていない。ひとつの方法論で研究者が必要とする全ての糖鎖を準備することは難しいであろう。そこで、複数の合成手法を活用することで、実用的な糖鎖ライブラリーを構築することが望ましいと筆者は考えている。

細胞を用いた糖鎖合成法　ー糖鎖プライマー法ー

細胞機能を利用して糖鎖ライブラリーを構築する手法の概略について述べる。細胞は糖鎖を合成している工場である。遺伝情報から翻訳された糖鎖合成酵素は、小胞体やゴルジ装置に局在し、糖脂質や糖タンパク質の糖鎖を合成している。例えば図1に示すように、糖脂質の場合には、セラミドにグルコース、次にガラクトースが結合してラクトシルセラミドになり、さらに複数の系列の糖脂質が合成される。ラクトシルセラミドに、シアル酸が結合するとガングリオ系列（NeuAcα2-3LacCer）、ガラクトースがα1-4で結合するとグロボ系列（Galα1-4LacCer）、ガラクトースがα1-3 で結合するとイソグロボ系列（Galα1-3LacCer）、*N*-アセチルグルコサミンがβ1-3 で結合するとラクト系列あるいはネオラクト系列（GlcNAcβ1-3LacCer）、などの糖鎖が生合成される。また*O*-グリカンでは、セリンにキシロースが結合するとプロテオグリカン鎖が、*N*-アセチルグルコサミンが結合すると糖タンパク質のムチン型糖鎖が伸長するようになる。このように、特定の糖鎖構造はその後に続く糖鎖伸長反応を決定する。このような特定の糖鎖構造をプライマー領域と呼ぶことができる。そこで、糖鎖生合成経路の基質となるプライマー領域の糖鎖を有するアルキルグルコシドを細胞に与えることで、糖鎖生合成経路を利用した糖鎖伸長生成物を得ることができる。筆者らは、このようなアルキルグルコシドを「糖鎖プライマー」と呼んでいる。

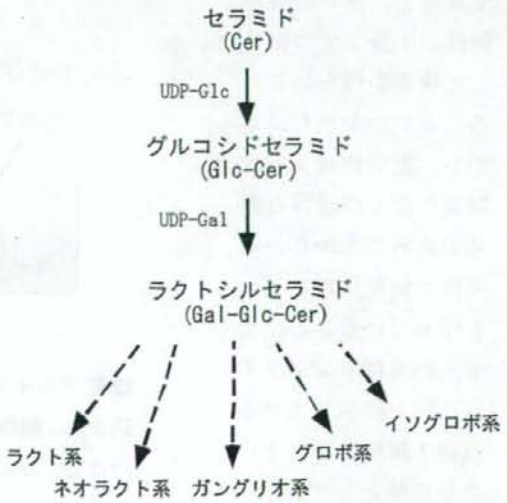

図1　糖脂質の生合成経路

例えば、ラクトシルセラミドは糖脂質の生合成経路の前駆体であり、その構造を模倣したドデシルラクトシドは糖鎖プライマーとしての機能を有している(5-7)（図2）。ドデシルラクトシドを培養液中に加えておくと、細胞内に取り込まれたのちゴルジにおいて糖鎖伸長を受ける。糖鎖伸長生成物は細胞外に分泌されるので、細胞を壊すことなく生成物を分離することができる。しかも、内在性の糖脂質に比べて、糖鎖プライマーから得た糖鎖伸長生成物は炭素鎖長が単一であるために構造解析が非常に容易である。糖鎖構造は、MALDI-TOF-MS/MS（マトリックス支援レーザーイオン化飛行時間型質量分析計）やESI-MS/MS（電子スプレーイオン化型質量分析計）などを用いて簡便に解析することができる。これにより微量な生成物の糖鎖の配列をより迅速に決定できるようになってきた。糖鎖プライマーに伸長した糖鎖構造を解析してみると、多くの場合糖鎖が1分子ずつ伸長した構造が得られていることがわかった。しかも、糖鎖伸長反応は糖鎖の生合成経路と同じであることから、内在性の糖脂質のコピーを作っていることになる。例えばガングリオa系列を発現しているCOS 7細胞にラクトースを糖鎖として有するプライマーを投与すると、GM3, GM2, GM1 およびGD1a型の糖鎖が同時に検出された（図2）。

細胞内で糖鎖伸長を受ける糖鎖プライマーの糖鎖や疎水基の構造には多様性がある。しかしながら、細胞内に取り込まれ、また生成物が細胞外に放出されるという性質を維持するには、適当な親疎水バランスが必要であることが見出されている(8)。例えば、ラクトシド以外にも、*N*-アセチルグルコサミンなどを有する糖鎖プライマーを用いることで、異なる系列のオリゴ糖鎖の伸長がみられることを明らかにしている。また野口研究所との共

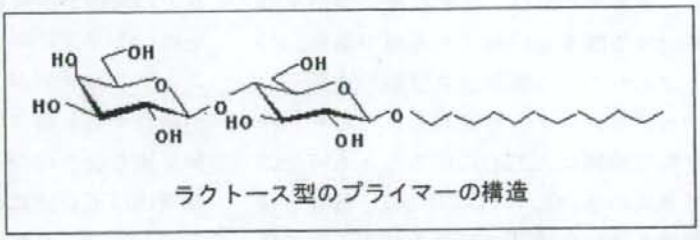

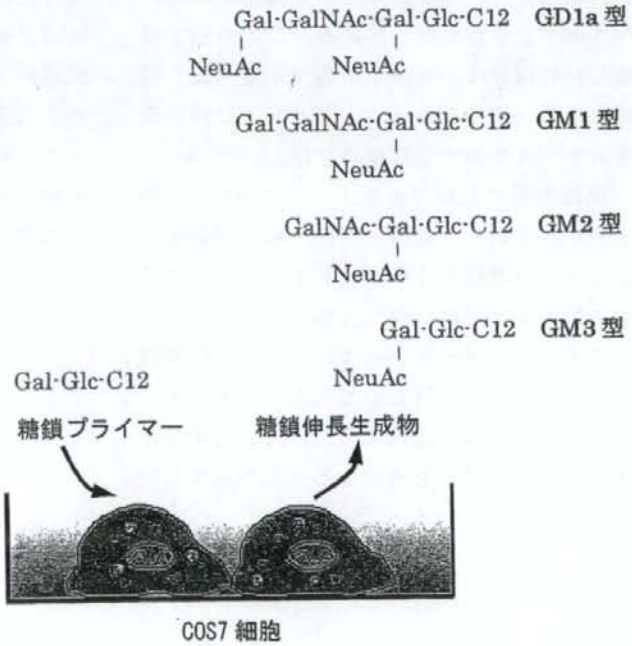

糖鎖プライマーを培地に投与すると細胞内に取り込まれ、細胞内の糖鎖生合成経路により糖鎖伸長を受ける。生成物は細胞外に分泌される。

図2　糖鎖プライマー法の原理

同研究によりムチン型の *O*-結合型糖鎖を得るための *N*-アセチルグルコサミンースレオニン結合体を親水基に有する糖鎖プライマーを開発することにも成功している。

筆者らの研究以外にも、細胞内での糖鎖生合成酵素の基質となるプライマーに関する研究が報告されている。例えば、β-D-Xyloside(9, 10)、GalNAcα-O-benzyl、Xylβ1-6Gal-O-2-naphthol、peracetylated Galβ1-4GlcNAcβ-O-naphthalenemethanol(11)、peracetylated Galβ1-4GlcNAcβ-O-naphthalenemethanol(12) は細胞内でのプロテオグリカンや糖タンパク質の糖鎖伸長反応の基質になり、細胞内の糖鎖生合成の阻害剤としても機能することが報告されている。アグリコンに benzyl 基や naphthyl 基を有したプライマーでは疎水性が高いために細胞内にとどまる傾向があるので、糖鎖伸長生成物は細胞を壊して分離する必要がある。それに対して、筆者らが用いているドデシルグルコシドでは、細胞内にとどまる能力が乏しいので、細胞内で糖鎖伸長された生成物は細胞外に分泌されることになる。そこで、糖鎖伸長生成物は細胞を分解することなく分離することができるので、我々が用いている糖鎖プライマーは糖鎖合成という点において利点がある。また、ドデシルグルコシドは糖脂質の生合成経路の基質であることが従来のプライマーとは異なる点である。

バイオコンビナトリアル合成法による糖鎖ライブラリーの作製

核酸やペプチドのライブラリーから機能性分子を探索することは、既に多くの研究者の重要な技術の一つになっている。一方、糖鎖の研究では有用な糖鎖ライブラリーがないことから、同様な探索研究を行うことは困難である。有機化学的な手法によるライブラリーの構築では、コンビナトリアルケミストリーの概念が用いられている。細胞を用いたオリゴ糖鎖の合成においても、同様の概念を利用することができる。この場合の組み合わせは「糖鎖プライマー」と「細胞」である。糖鎖プライマーは糖鎖生合成経路に応じて分子設計することができ、糖鎖を作り出している動物細胞の種類も膨大である。動物細胞以外の細胞でも利用することは可能であろう。図3に示すように、細胞と糖鎖プライマーを掛け合わせることで、細胞が合成できる多くのオリゴ糖鎖を作り出すことができる。これが、筆者らが提案している「バイオコンビナトリアル合成法」の原理である。

マウスメラノーマ細胞B16では主にガング

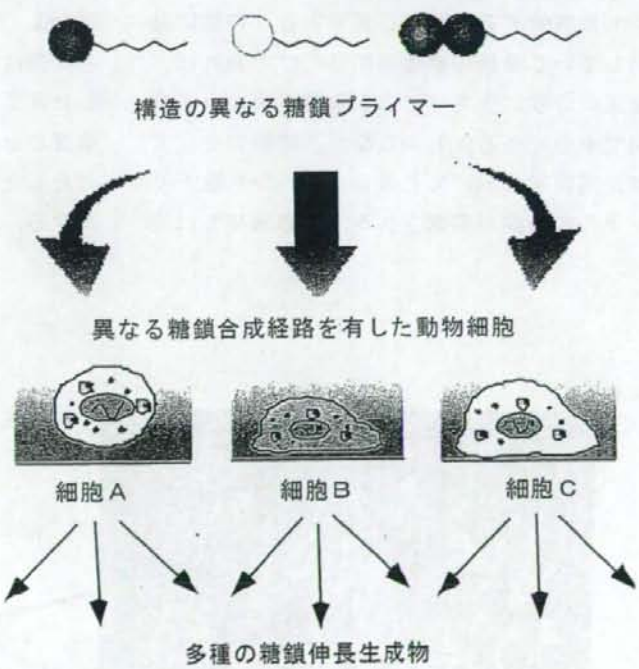

糖鎖プライマーと細胞の組合せにより細胞が合成できる種々のオリゴ糖鎖を得ることができる。
→　糖鎖ライブラリーの構築

図3　バイオコンビナトリアル合成法の原理

リオシドGM3、アフリカミドリザル腎臓細胞COS7ではガングリオa系列（GM3、GM2、GM1、GD1a）、ラット副腎髄質褐色細胞腫細胞PC12ではグロボ系列（Gb3）、ヒト前骨髄性白血病細胞 HL60 やヒト結腸がん細胞COLO201は、血液型抗原や細胞の接着因子として知られるシアル化ルイスXなどが含まれるネオラクト系列の糖鎖を発現している。このような細胞を用いて、糖鎖プライマーを投与することで、これまでに50種類以上の糖鎖伸長生成物を得ている。細胞の種類を増やすことでライブラリーの種類を増やすことが可能である。さらに大量培養を行うことで発現量の少ないオリゴ糖鎖の合成も検出できるようになっている。今後、糖脂質や糖タンパク質の糖鎖を約100種類合成することを目標に研究をすすめている。

細胞を用いて糖鎖の生産を行うには、細胞を大量培養する技術が必要である。細胞に発現している糖鎖の構造を知るだけであれば、通常の培養フラスコによる単層培養か浮遊培養で十分である。しかしながら糖鎖の生産では、実験室においても数リットルから数十リットルの培養が要求される。浮遊培養では培養液を増やすことでスケールアップすることは比較的簡単であるが、単層培養では培養フラスコをたくさん重ねる必要がある。この方法だと、培養に関わる労力が大きすぎる。それを解決するのが高密度培養法のひとつであるマイクロキャリア法である。これは市販のマイクロキャリアに細胞を接着させ、培養液中に懸濁させて培養する方法である。図4にマイクロキャリアに接着させた細胞の様子を観察した顕微鏡写真を示している。DEAEデキストランやコラーゲンで被覆したビーズが市販されており、細胞の種類に応じて使い分けることができる。筆者らが現在用いている条件でマイクロキャリア法と単層培養法での細胞数を比較すると、マイクロキャリア法での200mLの培養ボトル1本は10cm径の培養皿100枚に相当する。サンプルの投与、生成物の回収、培地交換などに関わる手間は200mLの培養ボトルも10cmの培養皿でも大きな差はない。糖鎖プライマー法では、生成したオリゴ糖鎖は培地中に存在するために、培養液を回収したあと、マイクロキャリアに付着した細胞は何度も繰り返して使うことができる。このように、マイクロキャリア法に

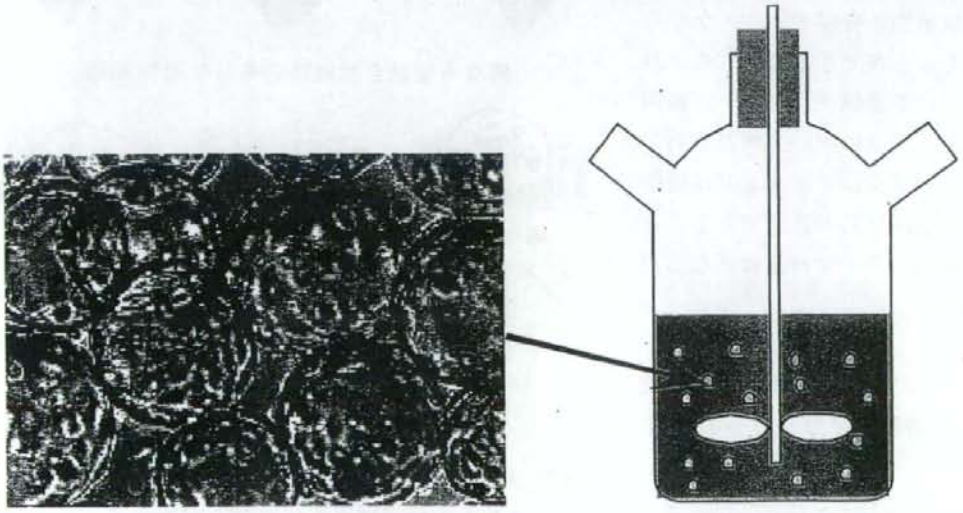

図4　マイクロキャリア法を用いた大量培養法

よる簡便な大量培養により糖鎖の合成を行うことができる。

今後のオリゴ糖鎖の生産には、生成物を分離・精製する技術を改良していく必要がある。細胞によっては構造の少し異なる糖鎖を多種類合成しているので、それらを簡便に迅速に分離することは糖鎖ライブラリーを効率よく生産するために必要な技術となるであろう。

グリコーム解析

糖鎖プライマー法では、糖鎖生合成経路が知られていない細胞でも当然ながら利用することができる。その場合にはプライマーへの糖鎖伸長反応により発現している糖転移酵素の存在や生合成経路を知ることができる。また、分化誘導における糖鎖構造の変化を追跡することにも利用している。HL60 細胞ではレチノイン酸などで誘起される分化誘導により、生合成される糖脂質の構造が変化することが知られている。そのような糖鎖合成経路の変化を、糖鎖プライマー法により検出することが可能であった。内在性の糖脂質の糖鎖構造を調べるのに比べて、簡便でしかも高感度な分析ができることが糖鎖プライマー法の特徴である。さらには、細胞を破壊することなく、継時的あるいは連続的なモニタリングを行うこともできる。また、糖鎖伸長生成物の構造解析により、プライマーへの糖鎖伸長に関わる糖転移酵素の発現を知ることができる。このように、糖転移酵素の存在と発現しているオリゴ糖鎖の配列を簡便に迅速に測定するグリコーム解析の手法としても利用できる。

糖鎖アレイ

糖鎖のマイクロアレイの開発のための基礎研究は 2002 年以降急速に増えてきている(13-16)。生体中のオリゴ糖鎖の研究が進んできたとはいえ、抗原、受容体、あるいは細胞間相互作用に関与している糖鎖の機能の全貌を明らかにしたわけではない。あるいは、オリゴ糖鎖が予想もしていないような分子と相互作用している可能性もある。糖鎖アレイが完成すれば、増殖、分化、転写など細胞機能に関与した生体分子との相互作用を幅広く簡便に検出することができるであろう。また、感染に関わる糖鎖構造の詳細を調べ直すこともできる。

そのためには、特に高等生物に発現しているオリゴ糖鎖をできるだけ多種類準備して、それを基板に簡便に固定化する技術が要求されることになる。これまでに、オリゴ糖鎖の基板への固定化は物理的吸着もしくは化学的な共有結合により行われている。筆者らは、前述したように糖鎖ライブラリーを作製する方法論の開発を行ってきた。そこで、次に、糖鎖プライマー法に適応可能な固定化技術について検討した。このような実験のために、12-azidododecyl lactoside（Lac-C12-N3）を用いた。このプライマーは、Lac-C12 と同様に細胞内で糖鎖伸長を受けるので、アジド基を有した糖鎖伸長生成物を得ることができる

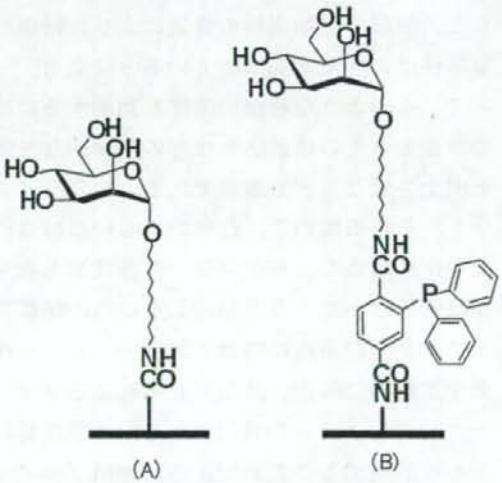

図5　アジド化糖鎖の基板への固定化。(A)アミンに還元したのち縮合反応で固定化。(B)トリフェニルホスフィン誘導体をリンカーとし Staudinger 反応で固定化。

(17)。アジド基を有したアルキルグルコシドは次の二つの方法で基板への固定化を行った。ひとつは、アジド基をアミノ基に還元して縮合する方法であり、もうひとつはトリフェニルホスフィン誘導体をリンカーとしてStaudinger 反応により固定化する方法である（図５）。いずれの方法でも固定化した糖鎖はレクチンや抗体分子と特異的な結合を検出することができた(18)。B16 細胞を用いて合成したNeuNAcα2-3Lac-C12-N3 を基板に固定化して、抗 GM3 抗体の結合を定量的に検出することにも成功している。多くの糖鎖アレイでは、糖鎖を固定化する際に官能基を共有結合するプロセスが必要であった。これに対して、固定化するオリゴ糖鎖の化学的な変換を不要もしくは簡便にすることがアジド化糖鎖プライマーを用いることで達成された。

おわりに

生体内で発現しているオリゴ糖鎖は、細胞の機能、細胞間相互作用、および各種疾病に関与しており、糖鎖の機能を理解することで病気の診断や治療に新たな道を開くことができる。糖鎖の生物機能の解析により、糖鎖の重要性はますます高まっていると言える。一方で、そのような糖鎖の機能を利用するには糖鎖合成とその修飾法等などの化学的な技術を向上させることも重要である。糖鎖ライブラリーを作るために、化学的あるいは酵素的な手法に加えて、細胞を用いた合成法も有用な技術になってくると期待している。糖鎖ライブラリーの用途は糖鎖センサーとしての検出や定量的な解析、糖鎖アレイによるスクリーニングシステムの開発、あるいは医用材料として活用することができる。糖鎖プライマー法は、従来の糖鎖合成法に加え新たな糖鎖ライブラリーの供給方法として利用できると期待している。

本研究の一部は、生物系特定産業技術研究推進機構（生研機構）のプロジェクト「細胞に作らせる糖鎖ライブラリーと機能性糖鎖高分子」および慶應義塾大学 21 世紀ＣＯＥプログラム「システム生物学による生命機能の理解と制御」として行われた。

文献

1. Zang, Z., Ollman, I., Ye, X., Wischnat, R., Baasov, T., and Wong, C. (1999) J. Am. Chem. Soc. **121**, 734-753
2. Plante, O. J., Palmacci, E. R., and Seeberger, P. H. (2001) Science **291**, 1523-1527
3. Murata, T., and Usui, T. (2006) Biosci. Biotech. and Biochem. **70**, 1049-1059
4. Narimatsu, H. (2004) Glycoconjugate J. **21**, 17-24
5. Miura, Y., Arai, T., and Yamagata, T. (1996) Carbohydr. Res. **289**, 193-199
6. Miura, Y., and Yamagata, T. (1997) Biochem. Biophys. Res. Commun. **241**, 698-703
7. Nakajima, H., Miura, Y., and Yamagata, T. (1998) J. Biochem. **124**, 148-156
8. Sato, T., Hatanaka, K., Hashimoto, H., and Yamagata, T. submitted to TIGG
9. Okayama, M., Kimata, K., and Suzuki, S. (1973) J. Biochem. (Tokyo) **74**, 1069-1073
10. Schwartz, N. B., Galligani, L., Ho, P.-L., and Dorfman, A. (1974) Proc. Natl. Acad. Sci., U.S.A. **71**, 4047-4051
11. Sarkar, A. K., Fritz, T. A., Taylor, W. H., and Esko, J. D. (1995) Proc. Natl. Acad. Sci. U. S. A. **92**, 3323-3327
12. Sarkar, A. K., Rostand, K. S., Jain, R. K., Matta, K. L. and Esko, J. D. (1997) J. Bio. Chem. **272**, 25608-25616
13. Fukui, S., Feizi, T., Galustian, C., Lawson, A. M., and Chai, W. (2002) Nature Biotech. **20**, 1011-1017
14. Houseman, B. T. and Mrksich, M. (2002)

Chem. Biol. **9**, 443-454

15. Park, S., and Shin, I. (2002) Angew. Chem. Int. Ed. **41**, 3180-3182
16. Blixt, O., Head, S., Mondal, T., Scanlan, C., Huflejt, M. E., Alvarez, R., Bryan, M. C., Fazio, F., Calarese, D., Stevens, J., Razi, N., Stevens, D. J., Skehel, J. J., van Die, I., Burton, D. R., Wilson, I. A., Cummings, R., Bovink, N., Wong, C-H, and Paulson, J. C. (2004) Proc. Natl Acad. Sci., U.S.A. **49**, 17033-17038
17. Kasuya, M. C. Z., Wang, L. X., Lee, Y. C., Mitsuki, M., Nakajima, H., Miura, Y., Sato, T., Hatanaka, K., Yamagata, S., and Yamagata, T. (2000) Carbohydr. Res. **329**, 755-763
18. Sato, T., Fujita, S., Kasuya, M. C. Z., Hatanaka, K., and Yamagata, T. (2004) Chem. Lett. **33**, 580-581

Specific Binding of GM1-Binding Peptides to High-Density GM1 in Lipid Membranes

Teruhiko Matsubara,[†] Kazutoshi Iijima,[†] Miwa Nakamura,[‡] Takao Taki,[§] Yoshio Okahata,[‡] and Toshinori Sato*,[†]

Department of Biosciences and Informatics, Keio University, 3-14-1 Hiyoshi, Kouhoku-ku, Yokohama 223-8522, Japan, Department of Biomolecular Engineering, Tokyo Institute of Technology, 4259 Nagatsuta, Midori-ku, Yokohama 226-8501, Japan, and Molecular Medical Science Institute, Otsuka Pharmaceutical Co. Ltd., 463-10 Kagasuno, Kawauchi, Tokushima 771-0192, Japan

Received July 3, 2006. In Final Form: September 4, 2006

The ganglioside Galβ1−3GalNAcβ1−4(Neu5Acα2−3)Galβ1−4Glcβ1−1'Cer (GM1) is an important receptor. We have previously identified GM1-binding peptides based on affinity selection from a random peptide library. In the present study, we determined the amino acids essential for binding GM1 and investigated the specific interaction with GM1 in the lipid membrane. Arginines and aromatic amino acids in the consensus sequence (W/F)RxL(xP/Px)xFxx(Rx/xR)xP contributed to the ability of the peptides to bind GM1. The peptide p3, VWRLLAPPFSNRLLP, having the consensus sequence, showed high affinity for GM1 with a dissociation constant of 1.2 μM. Furthermore, the density-dependent binding of p3 was investigated using mixed monolayers of GM1 and Glcβ1−1'Cer (GlcCer). p3 binds preferentially to high-density GM1, and its interaction with GM1 was found to be cooperative based on a Hill plot. These results indicated that a lateral assembly of GM1 molecules was required for the recognition of carbohydrates by p3. The GM1-binding peptide played a role as a unique anti-GM1 probe differing from the cholera toxin B subunit or antibodies.

Introduction

It has been reported that the lateral assembly of glycosphingolipids (GSLs) in the cell membrane is strongly related to their functions. The GSL-enriched microdomain (GEM) containing GSLs, cholesterol, phospholipids, and signaling proteins has been separated as a low-density detergent-insoluble membrane fraction by density gradient centrifugation.[1−3] The GEM in the plasma membrane is considered to be involved in cell−cell communication, signal transduction, and carbohydrate recognition. When the microdomain containing Galβ1−3GalNAcβ1−4(Neu5Acα2−3)Galβ1−4Glcβ1−1'Cer (GM1) was disrupted by the removal of cholesterol using β-cyclodextrin, the internalization of cholera toxin into cells was inhibited.[4] The gathering of GM1 was also related to the formation of fibrils by β-amyloid.[5,6] The notion that GEM plays crucial roles in the expression of carbohydrate functions has been widely accepted.

The lateral distribution of GSLs in the reconstituted membrane has been studied using air−water interface monolayers and vesicles.[7−9] Hashizume et al. carried out a quantitative analysis of the binding of lectin to GSL-containing lipid membranes and indicated that extensive affinity for lectin was induced by the phase-separation of GSLs in the membrane.[10] Recently, an atomic force microscope (AFM) has been employed to directly observe the topology of lipid membranes. AFM has a nanometer-scale lateral resolution and can visualize the lipid microdomains in membranes. Yuan and Johnston have reported that GM1-rich microdomains with a diameter of 30−200 nm were formed in the phospholipid membrane.[11,12]

Carbohydrate-binding proteins recognize terminal sugar residues of glycoconjugates.[13−15] For example, the cholera toxin B subunit (CTB) interacts with the terminal galactose and sialic acid of GM1, and this selectivity is achieved by a combination of hydrogen bonding and van der Waals interactions.[16] Peptide fragments of lectins could also bind to sugar chains, though with less specificity and selectivity than the parent proteins.[17,18] Peptides that bind to glycoconjugates such as carbohydrate antigens would be useful for the treatment of sugar-related diseases.[19] We developed a method of selecting GSL-binding peptides from a phage-displayed random peptide library using an air−water interface monolayer.[20] The GSL molecules are aligned in a lipid monolayer, and only hydrophilic sugar residues are exposed to the water phase. Since phage particles interact with only the sugar moiety of a GSL in an affinity selection process, nonspecific interaction between phage particles and the

* Corresponding author. E-mail: sato@bio.keio.ac.jp.
† Keio University.
‡ Tokyo Institute of Technology.
§ Otsuka Pharmaceutical Co. Ltd.

(1) Iwabuchi, K.; Handa, K.; Hakomori, S. *J. Biol. Chem.* **1998**, *273*, 33766.
(2) Iwabuchi, K.; Yamamura, S.; Prinetti, A.; Handa, K.; Hakomori, S. *J. Biol. Chem.* **1998**, *273*, 9130.
(3) Iwabuchi, K.; Zhang, Y.; Handa, K.; Withers, D. A.; Sinay, P.; Hakomori, S. *J. Biol. Chem.* **2000**, *275*, 15174.
(4) Orlandi, P. A.; Fishman, P. H. *J. Cell Biol.* **1998**, *141*, 905.
(5) Kakio, A.; Nishimoto, S. I.; Yanagisawa, K.; Kozutsumi, Y.; Matsuzaki, K. *J. Biol. Chem.* **2001**, *276*, 24985.
(6) Kakio, A.; Nishimoto, S.; Kozutsumi, Y.; Matsuzaki, K. *Biochem. Biophys. Res. Commun.* **2003**, *303*, 514.
(7) Maggio, B. *Prog. Biophys. Mol. Biol.* **1994**, *62*, 55.
(8) Luckham, P.; Wood, J.; Swart, R. *J. Colloid Interface Sci.* **1993**, *156*, 173.
(9) Luckham, P.; Wood, J.; Froggart, S.; Swart, R. *J. Colloid Interface Sci.* **1993**, *156*, 164.
(10) Hashizume, M.; Sato, T.; Okahata, Y. *Chem. Lett.* **1998**, 399.
(11) Yuan, C. B.; Furlong, J.; Burgos, P.; Johnston, L. J. *Biophys. J.* **2002**, *82*, 2526.
(12) Yuan, C. B.; Johnston, L. J. *Biophys. J.* **2001**, *81*, 1059.
(13) Lis, H.; Sharon, N. *Chem. Rev.* **1998**, *98*, 637.
(14) Weis, W. I.; Drickamer, K. *Annu. Rev. Biochem.* **1996**, *65*, 441.
(15) Quiocho, F. A. *Pure Appl. Chem.* **1989**, *61*, 1293.
(16) Merritt, E. A.; Sarfaty, S.; van den Akker, F.; L'Hoir, C.; Martial, J. A.; Hol, W. G. *Protein Sci.* **1994**, *3*, 166.
(17) Heerze, L. D.; Chong, P. C.; Armstrong, G. D. *J. Biol. Chem.* **1992**, *267*, 25810.
(18) Yamamoto, K.; Konami, Y.; Kusui, K.; Osawa, T. *FEBS Lett.* **1991**, *281*, 258.
(19) Peletskaya, E. N.; Glinsky, V. V.; Glinsky, G. V.; Deutscher, S. L.; Quinn, T. P. *J. Mol. Biol.* **1997**, *270*, 374.
(20) Matsubara, T.; Ishikawa, D.; Taki, T.; Okahata, Y.; Sato, T. *FEBS Lett.* **1999**, *456*, 253.

10.1021/la0619067 CCC: $37.00
Published on Web 11/22/2006

GSL-immobilized solid support was greatly excluded. In the present study, we investigated the amino acid residues contributing to the interaction between the peptide and GM1 by conducting a quantitative analysis using a quartz-crystal microbalance (QCM) and selective binding of the peptides to the GM1-enriched area in the lipid membrane using AFM.

Materials and Methods

Materials. The glycosphingolipids GM1, GalNAcβ1−4(Neu5Acα2−3)Galβ1−4Glcβ1−1′Cer (GM2), Galβ1−3GalNAcβ1−4Galβ1−4Glcβ1−1′Cer (asGM1), and Neu5Acα2−3Galβ1−3GalNAcβ1−4(Neu5Acα2−3)Galβ1−4Glcβ1−1′Cer (GD1a) from mink whale (*Balaenoputera* acutorostrata) were obtained from Prof. Kawanishi (Kitasato University, Japan). Neu5Acα2−3Galβ1−4Glcβ1−1′Cer (GM3) from bovine milk was obtained from Snow Brand Milk Products. Glcβ1−1′Cer (GlcCer), 1-palmitoyl-2-oleoyl-phosphatidylcholine (POPC), CTB, and peroxidase-conjugated CTB were purchased from Sigma.

Synthetic Peptides. The peptide amides (peptide-NH_2) were synthesized on an ACT357 automated peptide synthesizer from Advanced Chemtech using standard Fmoc chemistry. The crude peptide amides were purified by reversed-phase high-performance liquid chromatography, and then the purity and expected structure were verified by matrix-assisted laser desorption ionization/time-of-flight mass spectrometry (Voyger).

QCM Analysis. Lipid monolayers were prepared by the Langmuir−Blodgett technique. A lipid solution (chloroform/methanol = 2:1 or chloroform/ethanol = 4:1) (v/v) containing GSL (ca. 0.5 mg/mL) was spread on Tris-buffered saline (TBS) (50 mM Tris-HCl, 150 mM NaCl, pH 7.5) in a Teflon-coated Langmuir trough (USI System Co., Ltd.). The temperature in the subphase was held at 20 °C. A surface pressure−molecular area (π−A) isotherm was monitored using the Wilhelmy plate method. The GSL monolayer was compressed at a constant rate (10 cm^3 min^{-1}) and transferred horizontally to a gold surface of 27 MHz QCM (diameter 2.5 mm) at a surface pressure of 30 mN m^{-1}. The QCM was transferred to a handmade plastic tube filled with 1 mL of TBS, and the buffer was maintained at 20 °C with stirring. A peptide solution of 0.1 mM (or 1−10 mM) in TBS was added to the cuvette of the QCM, and the frequency decreases ($-\Delta F$, Hz) of the QCM responding to the addition of peptide were followed over time (Figure 1B). Each experiment was carried out 2−6 times. In the case of peptide binding, the calibration showed that a $-\Delta F$ of 1 Hz corresponded to a mass increase (Δm) of 0.91 ng cm^{-2} of peptide.[21,22] The Δm value (=amount of peptide bound) was plotted against the peptide concentration (Figure 1C). To obtain the dissociation constant (K_d) value, Δm was plotted against peptide concentration ([peptide]), and simple saturation curves indicating Langmuir adsorption were obtained (data not shown). Reciprocal plots between [peptide]/Δm and Δm gave straight lines according to the following equation

$$[\text{peptide}]/\Delta m = [\text{peptide}]/\Delta m_{max} + K_d/\Delta m_{max}$$

where Δm_{max} is the maximum amount of peptide that can bind and K_d is the dissociation constant. Δm_{max} and K_d were calculated from the slope and intercept of the linear relationship indicated by the equation, respectively. The Δm values of peptides p1, p2, and p3 were measured from 1 μM to 0.3 mM, 10 μM to 0.3 mM, and 1 to 10 μM, respectively, until no additional binding was observed. The obtained Δm_{max} values of p1, p2, and p3 were 124 ± 5, 112 ± 15, and 142 ± 1 ng cm^{-2}, respectively. In the case of CTB, a 9 MHz QCM (diameter 4.5 mm) was employed. The CTB solution (0.5 mg/mL, 8.6 μM) in TBS was added to the QCM cuvette (10 mL of TBS, final concentration was 5.1 nM). $-\Delta F$ of 1 Hz corresponded to Δm of 3.1 ng cm^{-2} of CTB.[22]

(21) Hoshino, Y.; Kawasaki, T.; Okahata, Y. *Biomacromolecules* **2006**, *7*, 682.

(22) Sato, T.; Serizawa, T.; Ohtake, F.; Nakamura, M.; Terabayashi, T.; Kawanishi, Y.; Okahata, Y. *Biochim. Biophys. Acta* **1998**, *1380*, 82.

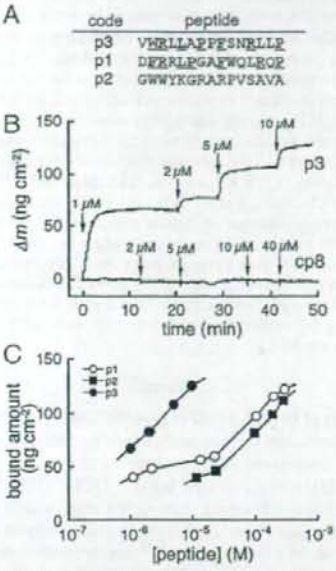

Figure 1. Quantitative analyses of GM1−peptide interactions using a QCM. (A) Amino acid sequence of GM1-binding peptides. The consensus sequence is in bold and underlined. (B) Typical time course of the mass increase of GM1-immobilized QCM, responding to the addition of peptides p3 and cp8 in TBS at 20 °C (pH 7.5). The arrows indicate the time of peptide injection and the final peptide concentration in a QCM cuvette. (C) Amounts of peptides bound to a GM1 monolayer as a function of peptide concentrations. p1, open circle; p2, closed square; p3, closed circle.

Competitive Inhibition Assay. A GM1 monolayer was prepared as described above and transferred to plastic plates (13.5 mm in diameter, Sumitomo Bakelite Co., Ltd.). The GM1-coated plates were blocked with 1% bovine serum albumin (BSA)/TBS overnight at 4 °C in 24-well multiple plates and then washed with 0.5 mL of TBS. The stock solution of a peptide was diluted with a horseradish peroxidase-conjugated CTB solution (1:5,000 dilution of 0.5% BSA/TBS) and then incubated with GM1-coated plates overnight at 4 °C. After three washes with TBS, the amount of CTB was determined by color development of orthophenylenediamine. When the fraction (f) of CTB-bound to GM1 was plotted against the concentration of competing peptide, sigmoidal curves were obtained. The binding fraction was defined as $f = B/B_{max}$, where B is absorbance at 492 nm due to the amount of CTB bound, and B_{max} is absorbance due to the maximum amount of CTB that can bind ([peptide] = 0). Then log [f/(1 − f)] was plotted against log [peptide] and the IC_{50} (50% inhibitory concentration) was calculated from the intercept (f = 0.5) of the plots.

AFM Measurement. The lipid bilayers were prepared as reported by Yuan et al. with minor revisions.[11] First, a POPC monolayer was prepared as described above using Milli-Q water as the subphase and transferred to the freshly cleaved mica by horizontal deposition at a surface pressure of 35 mN m^{-1} (POPC-coated mica). After drying overnight, another monolayer of GM1/GlcCer (10:90 or 90:10, mol %/mol %) was transferred to the POPC-coated mica by horizontal deposition at a surface pressure of 30 mN m^{-1}. AFM measurements were carried out on a SPA-300 (Seiko Instruments Inc.) in Milli-Q water at 25 °C. An FS20A scanner (scan area of 20 mm) and a cantilever (200-mm-long soft cantilevers with integrated pyramidal silicon nitride tips, spring constant of 0.02 N m^{-1}, SN-AF01, Olympus Optical Co., Ltd.) were used for all measurements. The typical scan rate was 1 Hz. After observation of the GM1/GlcCer membrane, the water was replaced with a p3 solution (1 or 10 μM). After incubation for 10 min, the peptide solution was again

replaced with water, and following two washes with water, the surface topology of the membrane was imaged in water.

Molecular Modeling. Molecular modeling was carried out with Insight II/Discover3 (Molecular Simulations Inc.). The initial secondary structure of p3 was predicted on the basis of the Chou and Fasman method.[23] Peptide was built using Biopolymer module of the Insight II program, and energy minimization was carried out. The molecular dynamics of the minimized structures were performed at 900 K for 2 ns without solvents, and 100 structures were collected after annealing at 298 K for 0.2 ns. The calculated structures were individual structures, but all of the molecules were globule, being 1.0−1.5 nm in diameter. A typical structure (0.9 nm × 1.7 nm × 2.7 nm) was used for the discussion on sugar recognition. The sugar structure of GM1 was obtained from the X-ray structural data of CTB (Protein Data Bank code, 3CHB). A circular dichroism spectrum suggested that p3 has no rigid structure in TBS (pH 7.5) (see Supporting Information), which was consistent with the result of molecular modeling.

Results

Binding of Peptides to Ganglioside GM1. The GM1-binding peptide sequences were identified in our previous study (Figure 1A).[20] In the present study, the binding of peptides (p1, p2, and p3) to GM1 was quantified using a QCM. QCM is a highly sensitive mass-measuring device, the resonance frequency of which decreases linearly with the increase in mass on a QCM electrode at the nanogram level.[22] An air−water interface GSL monolayer at a surface pressure of 30 mN m^{-1} was transferred onto a QCM electrode, and then the peptide solution was added to a QCM cuvette. Figure 1B shows the typical time course of mass increase (Δm), responding to the addition of p3 in the aqueous solution. This mass increase corresponds to the amount of peptide bound to GM1 immobilized onto a QCM electrode. The amount of p3 was saturated at $\Delta m = 70 \pm 4$ ng cm^{-2} within 20 min. The p3 concentration ranged from 1 to 10 μM, and corresponding binding was observed (Figure 1C). On the other hand, the addition of a control peptide (cp8) resulted in no increase, which means cp8 has no affinity for GM1 (Figure 1B).

From a reciprocal plot of [peptide]/Δm and Δm, the K_d values for p1, p2, and p3 were estimated to be 11 ± 3, 33 ± 4, and 1.2 ± 0.1 μM, respectively. The binding ability of p3 was about 10-fold greater than that of p1 and p2. This binding preference among the peptides was consistent with the results obtained in an inhibition assay, in which the IC_{50} values of p1, p2, and p3 were 24, 13, and 1.0 μM, respectively.[20]

Binding of Peptides to Various GSLs. The binding of p1, p2, and p3 to GM1, GM2, GM3, asGM1, GD1a, and GlcCer was examined with the QCM (Figure 2A). Typical binding curves are shown in Figure 2B, and the amount bound at 10 μM is summarized in Table 1. When the concentration of p3 was 10 μM, the amount of p3 bound to GM2 (57 ng cm^{-2}) or to asGM1 (82 ng cm^{-2}) was lower than that bound to GM1 (127 ng cm^{-2}), indicating that the terminal galactose and sialic acid of GM1 are required for the binding. On the other hand, p1 and p2 bound to other GSLs as well as GM1 (Table 1).

Arginines and Aromatic Amino Acids Are Essential for Binding GM1. The peptides p1 and p3 shared a consensus sequence, (W/F)RxL(xP/Px)xFxx(Rx/xR)xP (Figure 1A). Six kinds of synthetic peptide mutants were prepared to clarify the meaning of the consensus sequence. It was deduced that arginines (R) and aromatic amino acids (F and W) in the GM1-binding peptides cooperatively recognize sugars, because carbohydrate−protein interactions are usually mediated by a combination of hydrogen bonds and van der Waals interactions.[13−15] The affinity

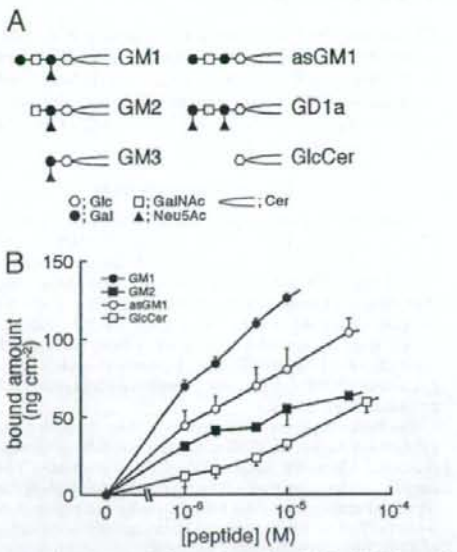

Figure 2. The binding of p3 to various glycolipids. (A) Schematic representation of gangliosides and GSLs. Glc, glucose; Gal, galactose; GalNAc, *N*-acetylgalactosamine; Neu5Ac, *N*-acetylneuraminic acid; Cer, ceramide. (B) Amounts of p3 bound to a GSL monolayer as a function of peptide concentrations. GM1, closed circle; asGM1, open circle; GM2, closed square; GlcCer, open square. Bars represent the SD ($n = 2-4$).

Table 1. Amounts of Peptides Bound to GSLs

peptide	GSL	bound amount[a] (ng cm^{-2})	relative amount[b]
p1	GM1	60 ± 3	1.0
	GM2	65 ± 19	1.1
	GM3	119 ± 30	2.0
	asGM1	26 ± 5	0.4
	GD1a	85 ± 25	1.4
	GlcCer	6 ± 2	0.1
p2	GM1	39 ± 0	1.0
	GM2	42 ± 4	1.1
	GM3	39 ± 4	1.0
	asGM1	45 ± 13	1.1
	GD1a	57 ± 6	1.5
	GlcCer	0 ± 0	0
p3	GM1	127 ± 3	1.0
	GM2	57 ± 12	0.4
	GM3	99 ± 18	0.8
	asGM1	82 ± 13	0.6
	GD1a	105 ± 2	0.8
	GlcCer	34 ± 4	0.3

[a] [peptide] = 10 μM. Values represent the mean ± SD ($n = 2-4$). [b] Ratio of the Δm for GM1 to that of each GSL.

of the peptide mutants for GM1 was estimated as the IC_{50} value, which is the concentration of the peptide that inhibits the binding of CTB to GM1 by 50%. CTB is well-known as a receptor of GM1 and has five B subunits that bind to the pentasaccharide moiety of GM1.[16] The IC_{50} value for p3 had been estimated to be 1.0 μM.[20] The IC_{50} values determined for the mutants are summarized in Table 2. The mutant p3RR in which Arg-3 and Arg-12 were replaced with Glu lost all ability to bind GM1 (IC_{50} > 500 μM). Since the two control peptides cpAR and cpLL containing two or three arginines showed no binding activity (IC_{50} > 500 μM), the position of the arginines in the peptides

(23) Chou, P. Y.; Fasman, G. D. *Annu. Rev. Biochem.* **1978**, *47*, 251.

Table 2. Inhibition Assay of Synthetic Peptides for CTB-Binding to GM1

code	substitution	amino acid sequence	IC_{50} (μM)	relative activity[a]
p3		H-VWRLLAPPFSNRLLP-NH_2	1.0[b]	1
p3RF	R3E, F9G	H-VW*E*LLAPP*G*SNRLLP-NH_2[c]	69	0.014
p3WR	W2G, R12E	H-V*G*RLLAPPFSN*E*LLP-NH_2	>500	<0.002
p3RR	R3E, R12E	H-VW*E*LLAPPFSN*E*LLP-NH_2	>500	<0.002
p3WF	W2G, F9G	H-V*G*RLLAPP*G*SNRLLP-NH_2	>500	<0.002
p3F	F9V	H-VWRLLAPP*V*SNRLLP-NH_2	6.0	0.17
p3P3	P7A, P8A, P15A	H-VWRLL*AAA*FSNRLL*A*-NH_2	0.68	1.5
cp8[d]		H-AEGDDPAKAAFDSLQ-NH_2	>500	
cp3[d]		H-AETVESCLAKPHTEN-NH_2	130	
cpAR		H-AREYGTRFSLTGGYR-NH_2	>500	
cpLL		H-LGRAGQSYPSFARGL-NH_2	>500	

[a] Ratio of the IC_{50} of p3 to that of each mutant. [b] From ref 20. [c] Substituted residues are bold and italic. [d] *N*-Terminal amino acids of major coat protein VIII (cp8) or minor coat protein III (cp3) of wild-type phages.

was important for the GM1 binding. The mutant p3WF, in which Trp-2 and Phe-9 were replaced with Gly, also completely lost the ability to bind GM1 (IC_{50} > 500 μM), whereas the mutant p3F, in which Phe-9 was replaced with Val, was only slightly affected (6.0 μM). These aromatic amino acids also contributed to the binding with GM1. The results of the point mutations indicated that the substitution of arginine (Arg-3 or Arg-12) and an aromatic amino acid (Phe-9 or Trp-2) resulted in a marked decrease in binding ability (IC_{50} of 69 μM for p3RF and > 500 μM for p3WR). Thus, it is considered that arginines and aromatic amino acids in the consensus sequence were closely involved in the recognition of the sugar moiety in GM1. Three prolines were found in the middle and at the carboxyl terminal end of p3. The IC_{50} value of 0.68 μM for a mutant p3P3, in which prolines were replaced with alanines, was almost the same as that for p3, and the binding activity of p3P3 was not changed significantly (Table 2).

Binding Affinity for GM1/GlcCer Membranes. The affinity of p3 for GM1/GlcCer mixed membranes was determined using the measurements made with the QCM. Figure 3A shows the time course of the binding (Δm, ng cm^{-2}) due to the frequency changes of the QCM at 1 μM of p3. Plots of the amount bound against the peptide concentration at 1−10 μM showed apparent saturation curves, and the amount of p3 depended on GM1 content (Figure 3B). Figure 4A shows the amount of p3 at 1 μM plotted against GM1 content. The amount of p3 increased exponentially in proportion to GM1 content, and the binding was observed at high GM1 levels (more than 80 mol %). This binding profile was analyzed with a Hill plot, because the Hill coefficient (n) gives the number of potential binding sites and is often used as a quantitative indicator of cooperative binding.[24]

$$M + nX \rightleftharpoons MX_n$$

Here M is p3 (or CTB) and X is GM1. From the Hill plot (Figure 4B), the n of p3 was determined to be 1.8, where the saturation fraction (p) was defined as 0 and 1 for the binding to 0% (=100% GlcCer) and 100% GM1, respectively. This n value suggested that p3 has two binding site. In other words, multiple GM1 molecules (more than one GM1 molecule) simultaneously bound to two binding sites of p3. To make comparisons with the properties of the GM1-binding peptide, the binding of CTB to GM1 was also examined. The amounts of CTB (5.1 nM) bound to GM1/GlcCer mixed membranes are shown in Figure 4A. The

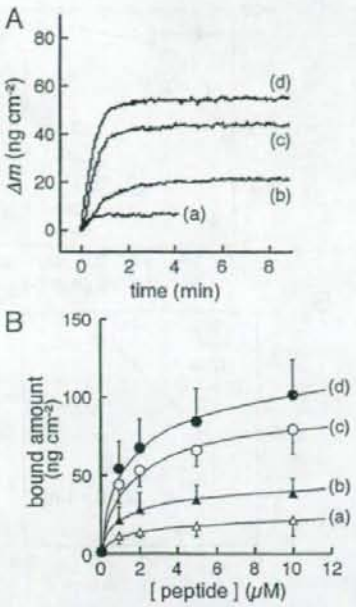

Figure 3. Quantitative analyses of p3 with GM1/GlcCer mixed membranes using a QCM. (A) Time courses of mass increase of GM1/GlcCer mixed monolayers, in response to the addition of p3 ([p3] = 1 μM). (B) Amounts of p3 bound to GM1/GlcCer mixed monolayers as a function of peptide concentrations. GM1/GlcCer = 10:90 mol % (a), 40:60 mol % (b), 80:20 mol % (c), and 90:10 mol % (d). Bars represent the SD (n = 2−4).

amount bound to GM1 showed a saturation curve against GM1 content. The Hill coefficient of CTB was 1.0, as shown in Figure 4B. An n value of 1.0 indicates that CTB has a single noninteracting binding site, meaning that each binding site equivalently binds to GM1, not cooperatively. That is, although CTB consists of five subunits, CTB behaves as a single unit.[25]

Direct Observation of Surface Topology by AFM. The GM1/GlcCer monolayer prepared with a Langmuir-type trough was transferred onto POPC-coated mica and the bilayer obtained was maintained in water. Then the surface topology of the bilayer in water was measured using an AFM. Since molecular modeling indicated that the height of GM1 was about 1 nm greater than that of GlcCer (data not shown), it was suggested that GM1 could be distinguished from GlcCer with an AFM. In fact, AFM measurements showed that the distribution of GM1 (light area, area A) was distinguishable from that of GlcCer (dark area, area C) in the case of the GM1/GlcCer (90:10 mol %) membrane (Figure 5A). Section analysis indicated that the difference in height between the GM1 and GlcCer areas was about 1.0−1.2 nm (Figure 5C, upper), which is consistent with the results of molecular modeling. In addition, an intermediate GM1 area having a height of 0.5 nm measured from the GlcCer area was also found (area B). These GM1 areas (A and B) were also found in 100 mol % GM1 membrane (data not shown). The existence of three heights (area A, B, and C) was also supported by the result of wave separation of the height histogram of the AFM image (data not shown). Area A was 50−500 nm in diameter. From a surface pressure−area isotherm, when GM1 molecules in the monolayer were highly ordered at a surface pressure of 30 mN

(24) Dahlquist, F. W. *Methods Enzymol.* **1978**, *48*, 270.

(25) Kuziemko, G. M.; Stroh, M.; Stevens, R. C. *Biochemistry* **1996**, *35*, 6375.

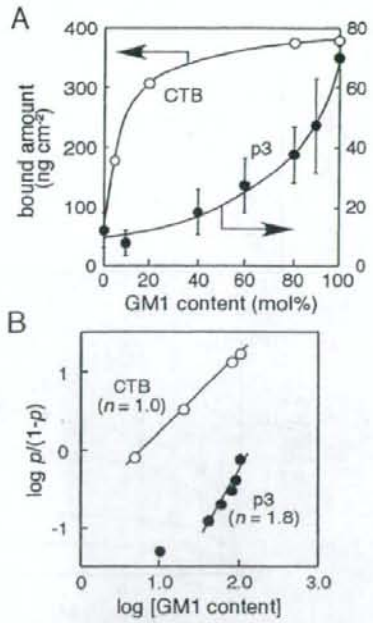

Figure 4. Binding of p3 and CTB to GM1/GlcCer membranes. (A) Amount of p3 at 1.0 μM (closed circle) and CTB at 5.1 nM (open circle) bound to GM1/GlcCer-mixed monolayers as a function of GM1 content (mol %). (B) Hill plots of p3 (closed circle) and CTB (open circle) against the concentration of GM1. The amounts at GlcCer and GM1 membranes are defined as a saturation fraction (p) of 0 and 1, respectively. n is the Hill coefficient.

m^{-1}, the occupied area of GM1 was 0.67 nm^2 per molecule (data not shown). For example, the number of GM1 molecules in a domain 50 nm in diameter is calculated to be 2,900.

For the detection of peptide−GM1 interaction, p3 (1 μM) was interacted with the GM1/GlcCer (90:10 mol %, Figure 5A) mixed membrane for 10 min. After the membrane's surface was washed with water, the surface topology was observed by AFM (Figure 5B). Section analysis indicated the appearance of the new layer 2.0−2.2 nm in height in area A (Figure 5C, lower). The increase in thickness corresponded to the size of p3. On the other hand, the surface of the GM1/GlcCer (10:90 mol %) membrane was smooth and the GM1 area was very small, and little binding of p3 (10 μM, excess concentration) was observed (see Supporting Information). The AFM images for the binding to the GM1/GlcCer membranes were well consistent with the results of the quantitative analysis by QCM (Figure 3).

Discussion

GSLs form a cluster with other lipids and signaling proteins in the plasma membrane.[26,27] The GSL cluster is also known as GEM. It has been reported that the binding of CTB to GEM leads to physiological events.[4] Since CTB binds specifically to the ganglioside GM1 in the plasma membrane during the initial internalization process, CTB has been used as a marker of GEM or lipid rafts.[4,28] It was also reported that the GM1 cluster induced the formation of fibrils of amyloid β-protein.[5,6] The cluster seems to provide an area for proteins to recognize. However, the recognizability of GEM has been little studied. Hashizume et al. proposed a methodology for quantitative measurements using a lipid monolayer.[10] An allo A lectin had high affinity for the lactosylceramide separated from dioleoylphosphatidylcholine in a mixed monolayer but had low affinity for the lactosylceramide homogeneously mixed with dipalmitoylphosphatidylcholine. That study provided the first quantitative evidence that the binding of the lectin depends on the distribution of GSL in the membrane.

We have employed a GM1 monolayer to select GM1-binding peptides from a phage-displayed random peptide library (Figure 1A).[20] One of the peptides identified, p3, showed the highest affinity for GM1. The amount of p3 bound to the GM1 monolayer increased depending on the concentration of peptide (Figure 1B,C). The amount was almost saturated when the peptide concentration was 10 μM. When the maximum amount was taken to be 142 ng cm^{-2}, the K_d of p3 was 1.2 μM. This K_d value was consistent with the IC_{50} value of p3, 1.0 μM, for CTB−GM1 interaction in our previous paper.[20] Lectins and antibodies have two or more sugar-binding sites to achieve multivalent effects. Although p3 was a 15-mer peptide, its binding affinity was comparable to the K_d values (0.4−1.7 μM) for the binding of concanavalin A to a maltose-bearing synthetic lipid.[29]

The binding selectivity of CTB has been reported to be GM1 > GM2 > GD1a > GM3 > GT1b > GD1b > asGM1 (surface plasmon resonance) or GM1 > GD1b > GM2 > GM3 > GT1b (radiolabeled immunoassay).[25] X-ray crystallographic data indicates that CTB interacts with a Neu5Ac (contribution to the interaction is 43%), a terminal Gal (39%), and a GalNAc (17%).[16] To identify sugar residues related to the recognition of the peptide p3, the selectivity of the peptides for six kinds of GSLs was studied. The amount of p3 bound to GSLs was GM1 > GD1a = GM3 > asGM1 > GM2 > GlcCer (Figure 2B and Table 1), which suggested that the terminal Gal and Neu5Ac in GM1 were concerned with the interaction as well as GSL recognition of CTB. The amino acid sequence of the selected peptide did not coincide with any protein involving CTB and lectins in the databases. Compared with the sequence of p1 and p3, a primitive similarity, (W/F)RxL(xP/Px)xFxx(Rx/xR)xP, was found (Figure 1A). The consensus sequence was composed of hydrophobic (Phe, Trp, Leu, and Pro) and cationic (Arg) amino acids. We focused on the preserved Arg, Phe, or Pro and synthesized six mutants (Table 2). The binding affinity of the mutants indicated that the arginines (Arg-3 and Arg-12) and aromatic amino acids (Trp-2 and Phe-9) cooperatively contributed to the recognition. In general, sugar-binding proteins recognize sugar residues through hydrogen bonds and hydrophobic stacking.[13,14] A guanidium group of arginine can interact with the ring oxygen and OH of sugar through hydrogen bonds and also can interact with the carboxylic acid of sialic acid through electrostatic interaction. An aromatic ring of Trp or Phe in galactose-binding lectins is stacked with the hydrophobic B-face of galactose. Furthermore, a methyl group of the acetoamido moiety in GlcNAc, GalNAc, or Neu5Ac often interacts with the aromatic ring of an amino acid. Therefore, Arg and aromatic amino acids in the consensus sequence should be reasonable candidates for amino acids interacting with GM1. On the other hand, in the case of CTB, His-13, Glu-11, Glu-51, Lys-91, and Asn-90 interact with Neu5Ac or the terminal Gal though hydrogen bonds.[16] In addition, Tyr-12 and Trp-88 interact with the terminal Gal and Neu5Ac through hydrophobic interaction, respectively. The molecular mechanism of sugar−peptide interaction may be the same for CTB and other sugar-binding proteins. For these reasons, it is

(26) Karlsson, K. A. *Annu. Rev. Biochem.* **1989**, *58*, 309.
(27) Varki, A. *Glycobiology* **1993**, *3*, 97.
(28) Brown, D. A.; Rose, J. K. *Cell* **1992**, *68*, 533.
(29) Ebara, Y.; Okahata, Y. *J. Am. Chem. Soc.* **1994**, *116*, 11209.

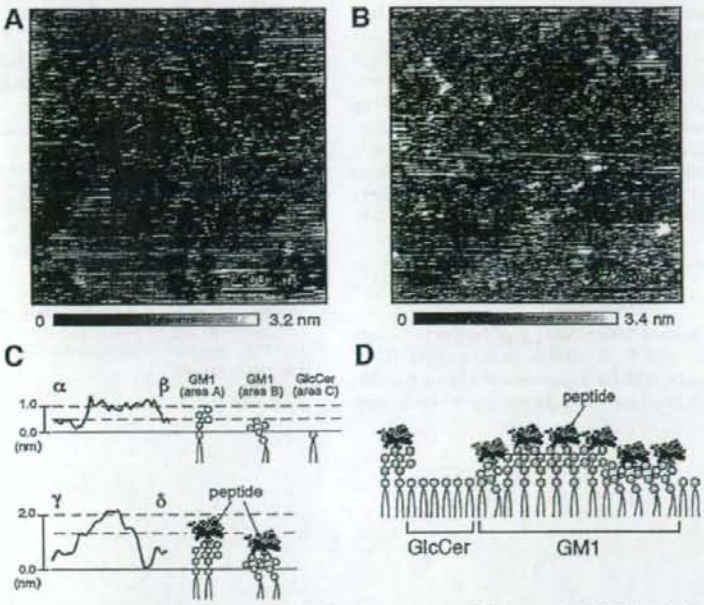

Figure 5. AFM images for studying the surface topology of GM1/GlcCer membranes. (A) Image of a GM1/GlcCer (90:10 mol %) membrane in water. The arrows indicate areas A, B, and C. (B) Image of a GM1/GlcCer (90:10 mol %) membrane after incubation with 1 μM of p3 for 10 min. (C) Typical section analysis plots and illustration of lipid membrane structure. The height of the GM1 area differed by 1.0−1.2 nm from that of the GlcCer area ($\alpha - \beta$, upper). The height of the GM1-peptide complex differed by 2.0−2.2 nm ($\gamma - \delta$, lower). (D) Schematic illustration of the binding of p3 to high-density GM1.

considered that the peptide−GM1 interaction was mediated by the interaction of Arg−Neu5Ac (or Arg−terminal Gal) and Trp/Phe−terminal Gal (or Trp/Phe−Neu5Ac).

Lipid monolayers have been employed to investigate the membrane structure and recognition function of GSLs.[22] In the present study, we investigated the binding of p3 to GM1/GlcCer mixed lipid monolayers with various amounts of GM1. GlcCer is a matrix lipid suitable for mixing with gangliosides, because p3 did not bind to GlcCer (Figure 2B and Table 1) and the headgroup of GlcCer did not disrupt lectin−ganglioside interaction.[22] The QCM-based analysis indicated that p3 showed no significant affinity for the mixed membrane containing 10 mol % or 40 mol % GM1 but bound extensively to the membrane containing more than 80 mol % GM1 (Figures 3 and 4). The Hill coefficient of 1.8 for the binding of p3 to the GM1/GlcCer membrane revealed that more than one GM1 molecule interacted with one p3 molecule (Figure 4). The molecular size of p3 was estimated to be 1.7 nm × 2.7 nm × 0.9 nm by computer modeling (Figure 6). The molecular area of the projected image of p3 (1.5−4.6 nm^2) corresponded to the area occupied by 2.3−6.8 GM1 molecules (0.67 nm^2 per GM1). Considering the molecular size of GM1 and p3, it is reasonable that p3 can bind to two GM1 molecules. In addition, if GM1 is mixed with other lipids by hexagonal packing, "GM1 pairs" (two neighboring GM1 molecules) form at high GM1 concentrations,[30] and the molecular area of GM1 increases exponentially with mole fraction.[31] Therefore, p3 could bind to high-density GM1 through a multivalent interaction.

The feature of p3 showing selective binding to high-density GSLs would be applicable for the detection of a nanometer-sized GSL cluster. The observation of GM1 membranes containing phospholipids, sphingolipids, and cholesterol with AFM indicated that GM1 forms a nanometer-sized cluster in the membrane.[11,12,32-35] The local density of GM1 in the cluster would be as high as 100 mol %. Thus, p3 was expected to preferentially bind to the GM1 cluster in the lipid membrane. To confirm the binding of p3 to the cluster, AFM technology was

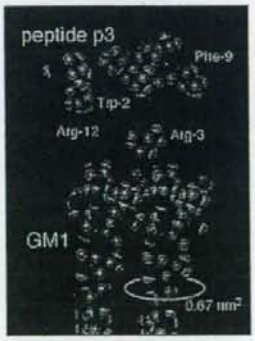

Figure 6. Model of p3 binding to GM1. The structure of p3 was predicted from molecular modeling, and that of GM1 was obtained from the Protein Data Bank (code 3CHB). The side chains of Trp-2, Arg-3, Phe-9, and Arg-12 are colored red.

(30) Massari, S.; Pascolini, D. *Biochemistry* **1977**, *16*, 1189.
(31) Carrer, D. C.; Maggio, B. *Biochim. Biophys. Acta* **2001**, *1514*, 87.
(32) Yokoyama, S.; Ohta, Y.; Sakai, H.; Abe, M. *Colloids Surf. B* **2004**, *34*, 65.
(33) Ohta, Y.; Yokoyama, S.; Sakai, H.; Abe, M. *Colloids Surf. B* **2004**, *33*, 191.
(34) Ohta, Y.; Yokoyama, S.; Sakai, H.; Abe, M. *Colloids Surf. B* **2004**, *34*, 147.
(35) Yuan, C.; Johnston, L. J. *Biophys. J.* **2000**, *79*, 2768.

employed. First, we observed the surface topology of 10 and 90 mol % GM1 membranes. Observations indicated that the surface of the 10 mol % GM1 membrane was smooth and no GM1 cluster was present (see Supporting Information). On the other hand, the surface of the 90 mol % GM1 membrane was heterogeneous with areas of GM1 and GlcCer (Figure 5A). When p3 at 1 μM interacted with the GM1/GlcCer (90:10 mol %) membrane, an increase in height of 1.0 nm was observed only in the GM1 area (areas A and B) and was approximately consistent with the size of p3 (0.9−2.7 nm) (Figure 5B,C). From these results, it was confirmed that p3 binds selectively to the GM1 cluster (Figure 5D). The peptide p3 is the first candidate for an artificial probe that recognizes GSL clusters.

Conclusion

We found a way to select GM1-binding peptides from a random peptide library. The peptide p3 showed an affinity for GM1, having a K_d of 1.2 μM, with the arginines and aromatic amino acids in p3 playing an important role in the binding. In experiments using mixed lipid monolayers, the peptide was found to bind preferentially to high-density GM1. AFM-based observations indicated that the peptide selectively recognized GM1 clusters in the lipid membrane. The binding behavior of the peptide was different from that of CTB. On the basis of these investigations, we carried out the development of an artificial lectin having the ability to recognize various glycolipids.

Acknowledgment. This study was partly supported by Special Coordination Funds for Promoting Science and Technology (14380411, T.S.) and by a Grant-in-aid for the Encouragement of Young Scientists (17750166, T.M.) from the Ministry of Education, Culture, Sports, Science and Technology of the Japanese Government.

Supporting Information Available: AFM images of GM1/GlcCer (10:90 mol %) membranes and circular dichroism spectrum of p3. This material is available free of charge via the Internet at http://pubs.acs.org.

LA0619067

RAPID COMMUNICATIONS IN MASS SPECTROMETRY
Rapid Commun. Mass Spectrom. 2007; 21: 191–198
Published online 15 December 2006 in Wiley InterScience (www.interscience.wiley.com) DOI: 10.1002/rcm.2825

RCM

The distinction of underivatized monosaccharides using electrospray ionization ion trap mass spectrometry

Xingyu Zhu and Toshinori Sato*
Department of Biosciences and Informatics, Keio University, 3-14-1 Hiyoshi, Yokohama 223-8522, Japan

Received 15 April 2006; Revised 30 October 2006; Accepted 8 November 2006

A convenient method for distinguishing underivatized isomeric monosaccharides has been established using electrospray ionization ion trap mass spectrometry (ESI-ITMS). Mass spectra of hexoses (glucose, galactose, and mannose), *N*-acetylhexosamines (*N*-acetylglucosamine, *N*-acetylgalactosamine, and *N*-acetylmannosamine) and hexosamines (glucosamine, galactosamine, and mannosamine) dissolved in solvent containing 1 mM ammonium acetate were obtained in the positive ion mode. Glucose was distinguished from galactose and mannose in the MS^2 spectrum of the $[M+NH_4]^+$ ion at *m/z* 198. The MS^3 spectra generated from $[M+NH_4-H_2O-NH_3]^+$ at *m/z* 163 showed that galactose and mannose could be distinguished by the ratio of peak intensities at *m/z* 145 and 127, while the three *N*-acetylhexosamine and hexosamine stereochemical isomers could be identified by the relative abundance ratios of product ions observed in MS^3 spectra. The investigation of MS and MS^2 spectra from complexes of these monosaccharides with Na^+ and Pb^{2+} failed to distinguish these monosaccharide isomers. Therefore, multiple stage mass analysis by ESI-ITMS using either $[M+NH_4]^+$ or $[M+H]^+$ was useful to distinguish between the isomers of monosaccharides.

An increasing number of reports have shown that oligosaccharides exhibit various important biological functions such as protein conformation, molecular recognition and cellular interaction.[1] Hexoses such as glucose (Glc), galactose (Gal), or mannose (Man), and *N*-acetylhexosamines such as *N*-acetylglucosamine (GlcNAc), *N*-acetylgalactosamine (GalNAc), or *N*-acetylmannosamine (ManNAc) are common monosaccharide units present in oligosaccharides conjugated to glycoproteins and glycolipids in mammalian physiology. Hexosamines such as glucosamine (GlcN), galactosamine (GalN), or mannosamine (ManN) are found in many biologically significant glycosaminoglycans.[2] Each class of diastereomeric monosaccharides has the same molecular weight (Fig. 1).

The first step in investigating the functions of oligosaccharides is structural elucidation that involves the identification of saccharide components, and determination of sequences.[3] Current methodologies such as permethylation/hydrolysis, periodate oxidation and enzymatic reduction[4] are used for carbohydrate analysis. Although nuclear magnetic resonance (NMR) spectrometry has been the standard tool in the structural analysis of carbohydrates,[5] recently, mass spectrometry, which can offer precise results and very high sensitivity, has been shown to contribute significantly to the structural aspects of glycobiology.[6]

Earlier investigations of carbohydrates by mass spectrometry (MS) were performed using acetyl and methyl derivatives,[4] and many studies on the structural elucidation of carbohydrates have been performed using fast-atom bombardment MS,[7] electrospray ionization (ESI)-MS),[8–16] and matrix-assisted laser desorption/ionization MS.[17] In particular, ESI-MS has evolved as a powerful analytical tool for the elucidation of oligosaccharide sequences, as well as the distinction of monosaccharide stereoisomers such as hexoses,[3,9–11] hexosamines,[8,12] and *N*-acetylhexosamines.[13–16,18]

Leary and coworkers have analyzed HexN derivatives[8] and HexNAc derivatives[16] chemically conjugated with metal complexes such as $[Co(DAP)_2Cl_2]Cl$, and performed the structural elucidation of hexose with $Zn(dien)_2Cl_2$ derivatives[3] and $Ni(NH_2(CH_2)_3NH_2)_3Cl_2$ derivatives.[10,11] Metal-hexose complexes such as $[Pb(monosaccharide)_m-H]^+$ ions $(m = 1–3)$[9] have been used to distinguish stereoisomers without derivatizating hexose. March and Stadey have reported that pentoses, hexoses and disaccharides were distinguishable using a quadropole time-of-flight tandem mass spectrometer combined with ESI.[19] The fragmentation mechanisms of protonated glucose, sucrose and fructose have been investigated using inductively coupled plasma (ICP) and ESI-MS.[20] A method for differentiating between flavonoid glucosides and flavonoid galactosides has been proposed using ESI-tandem mass spectrometry (MS/MS).[21]

**Correspondence to*: T. Sato, Department of Biosciences and Informatics, Keio University, 3-14-1 Hiyoshi, Yokohama 223-8522, Japan.
E-mail: sato@bio.keio.ac.jp
Contract/grant sponsor: Special Coordination Funds for Promoting Science and Technology from the Ministry of Education, Culture, Sports, Science and Technology, the Japanese Government.

RCM

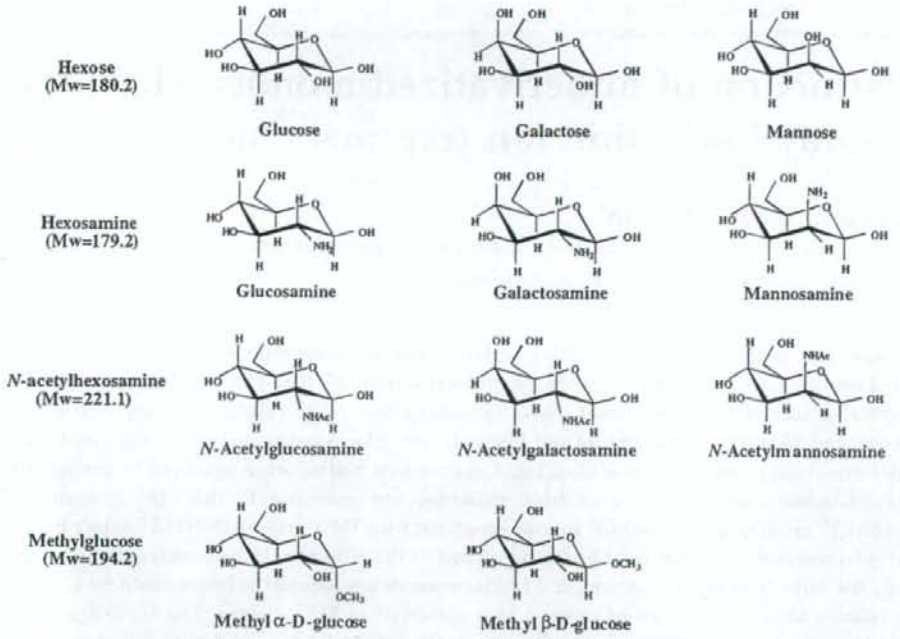

Figure 1. Chemical structures of the monosaccharide isomers used in this study.

Ammonium-cationized glucose, methyl α-D-glucopyranoside, and acetylated sugars have been investigated using chemical ionization mass spectrometry.[22] Collision-induced dissociation of ammonium-cationized α- and β-hexose peracetates has been studied for anomeric distinction.[23] A kinetic method based on proton affinity differences has been employed to differentiate diastereomeric hexosamines[12] and *N*-acetylhexosamines[14] with a triple quadrupole mass spectrometer.

In this study, we aimed to distinguish monosaccharide stereoisomers without derivatization using ion trap mass spectrometry (ITMS). First, we investigated the fragmentation patterns of monosaccharide isomers by adding sodium acetate solution to produce [monosaccharide +Na]$^+$ ions and lead(II) nitrate solution to generate [Pb(monosaccharide)$_m$–H]$^+$ ions as reported previously;[9] however, monosaccharide isomers could not be identified by MS^2 and MS^3 spectra obtained from monosaccharides complexed with either Na^+ or Pb^{2+} using ESI-ITMS. Next, the sequential stages of mass spectrometry (MS^n) of hexose isomers, methyl α-D-glucopyranoside and methyl β-D-glucopyranoside isomers, hexosamine isomers, and *N*-acetylhexosamine isomers were identified in the presence of 1 mM ammonium acetate. Hexoses could be distinguished from each other by MS^2 and MS^3 spectra in positive ion mode. Methyl α-D-glucopyranoside and methyl β-D-glucopyranoside isomers could be distinguished from each other by MS^2 spectra obtained both in positive and negative ion modes. Hexosamines and *N*-acetylhexosamines showed significant differences in the MS^3 fragment patterns detected in positive ion mode.

EXPERIMENTAL

Chemicals

D-glucose (Glc), D-galactose (Gal), D-allose (All), D-fructose (Fru), lead(II) nitrate, and sodium acetate were purchased from Wako (Osaka, Japan). D-Mannose (Man) was obtained from Nacalai Tesque, Inc. (Kyoto, Japan). Methyl α-D-glucopyranoside (MeαGlc) and methyl β-D- glucopyranoside (MeβGlc) were purchased from Tokyo Kasei Kogyo Co., Ltd. (Tokyo, Japan). D-Glucosamine hydrochloride (GlcN·HCl), D-galactosamine hydrochloride (GalN·HCl), D-mannosamine hydrochloride (ManN·HCl), *N*-acetyl-D-glucosamine (GlcNAc), *N*-acetyl-D-galactosamine (GalNAc), and *N*-acetyl-D-mannosamine (ManNAc) were purchased from Sigma-Aldrich (St Louis, MO, USA). The purities of the monosaccharides were 98–99%. Acetonitrile (for LC/MS) and methanol (for LC/MS) were purchased from Wako (Osaka, Japan). Water of the required purity for preparing monosaccharide standard stocks was obtained using a Milli-Q-water purification system (Millipore, USA).

Mass spectrometry

ESI-MS^n spectra were recorded using an ion trap mass spectrometer equipped with an ESI source (Esquire 3000 plus, Bruker, German). In positive ion mode, the entrance to the capillary was −4 kV relative to the needle and −500 V relative to the endcap. The spray was stabilized with nitrogen sheath gas operating at 10 psi, and drying gas heated at 250°C, and a flow rate of 4 L/min was used to evaporate solvent in the spray chamber. In MS^2 experiments, a mass range of *m*/*z* 50–270 was scanned. The width of isolation was

DOI: 10.1002/rcm

set to 4.0 and the fragmentation amplitude was set to 1.00 V in the 'smart fragmentation' mode.

Hexose (100 μM), MeαGlc (100 μM), MeβGlc (100 μM), hexosamine hydrochloride (10 μM), and *N*-acetylhexosamine (10 μM) were dissolved in acetonitrile/water (1:1, v/v) solvent supplemented with 1 mM ammonium acetate. The concentration of sodium ions was 10 μM, and the concentration of lead ions was 50 μM. In proton cationization, 0.1% acetic acid was added to the monosaccharide solution. All samples were injected for analysis by ESI-MS using direct infusion with a syringe pump at a flow rate of 4 μL/min after filtration with a 0.45 μm filter membrane (Millex, Millipore, USA).

RESULTS AND DISCUSSION

Distinction between Glc, Gal, and Man

The distinctions between Glc, Gal and Man dissolved in acetonitrile/water (1:1, v/v) solvent supplemented with 1 mM ammonium acetate were examined by ESI-MS (data not shown). The ions $[M+NH_4]^+$ at *m/z* 198 (base peak) and $[M+Na]^+$ at *m/z* 203 were detected in MS spectra. $[M+NH_4-NH_3]^+$ at *m/z* 181 was also detected at low abundance. Two in-source fragment ions at *m/z* 180 and 163 arising from the loss of one H_2O molecule from *m/z* 198 were also detected; the MS spectra of those isomers did not show any significant differences. By increasing the concentration of ammonium acetate, the intensity of $[M+NH_4]^+$ increased, but when the concentration of ammonium acetate was above 1 mM, the intensity of $[M+NH_4]^+$ showed a downward trend because excessive NH_4^+ decreased the overall sensitivity. On the other hand, $[M+NH_4-NH_3]^+$ at *m/z* 181 could not be used for MS^2 spectra, because its abundance was very low and it was difficult to isolate it from ions at *m/z* 180.

Next, the MS^2 spectra generated from $[M+NH_4]^+$ at *m/z* 198 showed product ions at *m/z* 181, 180, 163, 145, and 127 (Fig. 2(A)), which were considered to be $[M+NH_4-NH_3]^+$, $[M+NH_4-H_2O]^+$, $[M+NH_4-H_2O-NH_3]^+$, $[M+NH_4-2H_2O-NH_3]^+$, and $[M+NH_4-3H_2O-NH_3]^+$, respectively, according to the literature.[22] The product ion at *m/z* 181 could not be used for MS^3 spectra because its abundance was very low and it could not be separated from *m/z* 180.

In Fig. 2(A), the relative abundance of *m/z* 180 was larger than *m/z* 163 and 145 for Glc, while the product ion at *m/z* 163 showed the largest abundance for Gal and Man. The reproducibility of these results was confirmed by altering the fragmentation amplitude from 0.5 through 1.3 V (Fig. 2(B)). The relative abundance ratios of ions at *m/z* 180 and 163 for Glc were larger than 1 at every fragmentation amplitude, although those for Gal and Man were 0.05–0.3. The data showed the clear distinction of Glc from Gal and Man.

Since the MS^2 spectra of Gal and Man were almost identical, the MS^3 spectra were obtained to distinguish Gal and Man (Fig. 3). The ions at *m/z* 163 in the MS^2 spectra were selected to examine MS^3 spectra. A higher abundance of product ions $[M+NH_4-2H_2O-NH_3]^+$ at *m/z* 145, $[M+NH_4-3H_2O-NH_3]^+$ at *m/z* 127, and $[M+NH_4-H_2O-NH_3-C_2H_6O_3]^+$ at *m/z* 85 was detected for both Gal and Man, while the product ions $[M+NH_4-H_2O-NH_3-CH_4O_2]^+$ at *m/z* 115, $[M+NH_4-H_2O-NH_3-C_2H_4O_2]^+$ at *m/z* 103, $[M+NH_4-H_2O-NH_3-CH_6O_3]^+$ at *m/z* 97, and $[M+NH_4-H_2O-NH_3-C_3H_4O_2]^+$ at *m/z* 91 were only detected for Gal, and were considered to be generated by cross-ring cleavage reaction.[3,24] An obvious difference in the relative abundance ratio of *m/z* 145 to 127 between Gal and Man was observed from Fig. 3(A).

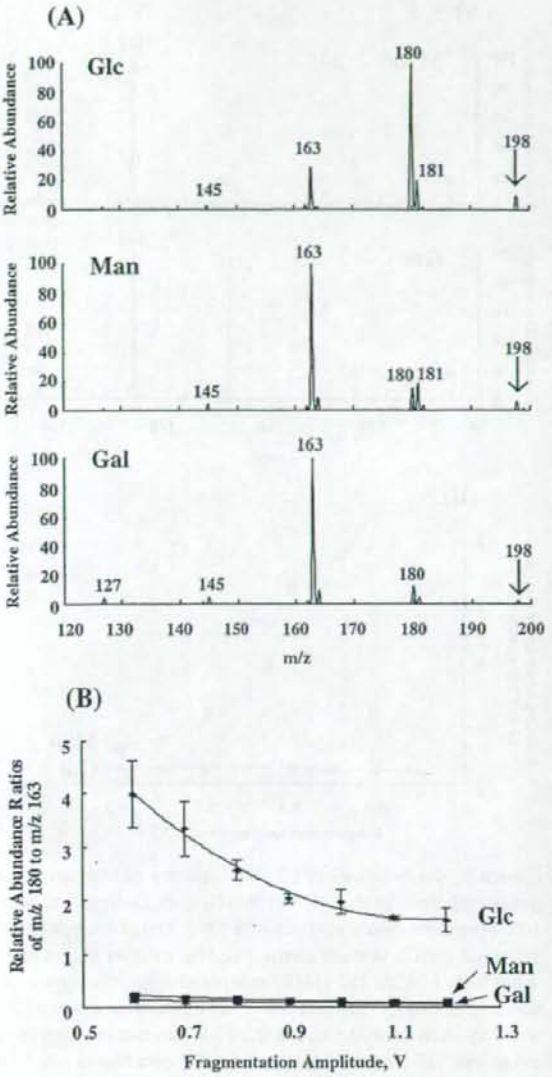

Figure 2. (A) Positive ion ESI-MS^2 spectra of Glc, Man, and Gal generated from precursor ion $[M+NH_4]^+$ at *m/z* 198. Fragmentation amplitude was 0.8 V. The precursor ion is indicated with a vertical arrow. (B) The relative abundance ratios of ions at *m/z* 180 to *m/z* 163 in MS^2 spectra at different fragmentation amplitudes for Glc, Man, and Gal. Two fragment ions at *m/z* 180 and 163 were detected above 0.6 V for the three isomers.

DOI: 10.1002/rcm

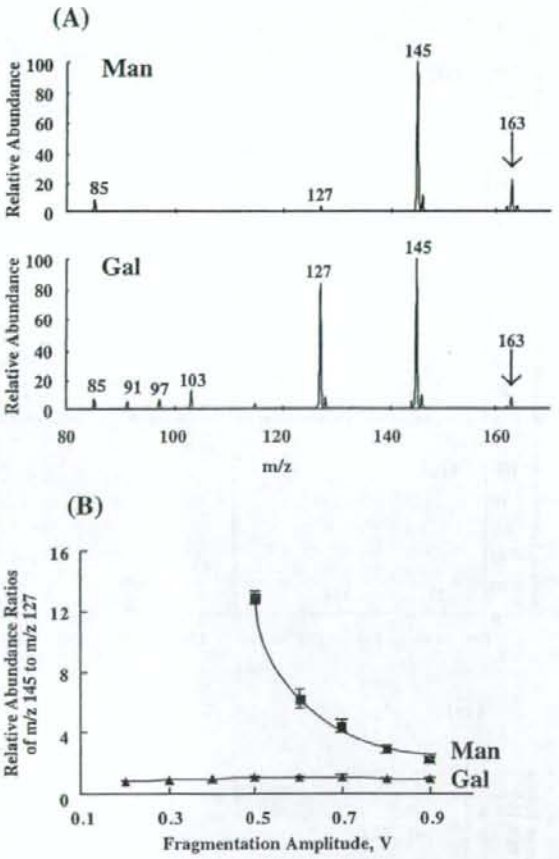

Figure 3. (A) Positive ion ESI-MS^3 spectra of Man and Gal generated from precursor ion $[M+NH_4-H_2O-NH_3]^+$ at *m/z* 163. Fragmentation amplitude was 0.5 V. The precursor ion is indicated with a vertical arrow. (B) The relative abundance ratios of *m/z* 145 to 127 in MS^3 spectra at different fragmentation amplitudes for Man and Gal. The fragment ions at *m/z* 127 and 145 were detected above 0.2 V for Gal, but the fragment ion at *m/z* 145 was detected above 0.4 V, and that at *m/z* 127 was detected above 0.5 V for Man.

The relative abundances at *m/z* 145 and 127 were measured by altering fragmentation amplitudes from 0.1 through 1.0 V (Fig. 3(B)). The abundance ratios of *m/z* 145 to 127 were larger than 2 and depended on the fragmentation amplitude for Man, although they were almost the same as for Gal. The data showed a clear distinction between Gal and Man.

These results showed that hexoses could be identified by MS^2 and MS^3 spectra of the $[M+NH_4]^+$ ions using ESI-ITMS. When hexoses were dissolved in acetonitrile/water (1:1, v/v) solvent supplemented with 0.1% acetic acid and examined by ESI-MS, $[M+H]^+$ at *m/z* 181 and $[M-H_2O+H]^+$ at *m/z* 163 (base peak) were detected in each MS spectrum. The abundance of the $[M+H]^+$ ions at *m/z* 181 was too low to obtain MS^2 spectra for Glc and Gal. No significant differences were observed in MS^2 and MS^3 spectra generated from $[M-H_2O+H]^+$ at *m/z* 163. Therefore, $[M+H]^+$ and $[M-H_2O+H]^+$ could not be used to distinguish the three hexose isomers.

Next, the fragmentation patterns of Na^+ additives were investigated. The mass spectra showed a single $[M+Na]^+$ ion at *m/z* 203 for hexoses dissolved in 10 μM sodium acetate. The MS^2 spectra mainly included product ions $[M-H_2O+Na]^+$ at *m/z* 185, $[M-C_2H_4O_2+Na]^+$ at *m/z* 143, and $[M-C_2H_6O_3]^+$ at *m/z* 102, and showed no significant difference between the three hexose isomers: Glc, Gal and Man (data not shown).

Furthermore, the MS^n spectra of hexoses dissolved in methanol/water (1:1, v/v) supplemented with 50 μM lead(II) nitrate were investigated according to the literature.[9] The base peak of $[Pb(hexose)-H]^+$ at *m/z* 387 was detected in MS spectra, so it was selected to examine MS^2 spectra. The product ions were detected above 0.4 V and the precursor ion disappeared at 0.6 V for Glc and Man, and at 0.7 V for Gal, respectively. The base peaks of the three isomers were $[Pb(hexose)-C_2H_4O_2-H]^+$ at *m/z* 327. This differs from the literature, where it has been reported, using an ESI-triple quadrupole mass spectrometer, that the base peak of Gal was $[Pb(hexose)-C_4H_8O_4-H]^+$ at *m/z* 267.[9] It is not unexpected that different results may be obtained given the differences in collision conditions on these two instruments. Next, the ion at *m/z* 327 was used to examine MS^3 spectra. Product ions $[Pb(hexose)-C_2H_6O_3-H]^+$ at *m/z* 309, $[Pb(hexose)-C_3H_8O_4-H]^+$ at *m/z* 279, and $[Pb(hexose)-C_4H_8O_4-H]^+$ at *m/z* 267 showed no difference between the three isomers, which could therefore not be distinguished using lead ion additives by ESI-ITMS.

This method was also applicable to distinguish Fru and All from other hexoses. $[Fru+NH_4]^+$ and $[All+NH_4]^+$ at *m/z* 198 were largely detected in MS spectra. MS^2 spectra produced from the precursor ion at *m/z* 198 showed product ions such as $[M+NH_4-H_2O]^+$ at *m/z* 180, $[M+NH_4-H_2O-NH_3]^+$ at *m/z* 163, and $[M+NH_4-2H_2O]^+$ at *m/z* 162 above a fragmentation amplitude of 0.6 V. The relative abundance ratios of *m/z* 180 to 163 were larger than 2 at fragmentation amplitude 0.6 through 1.2 V for Fru and All. The energy breakdown curves were similar to that of Glc, and were different from that of Gal and Man (data not shown). The relative abundance ratios of *m/z* 163 to 162 were almost 1 for All, and were larger than 3 for Fru and Glc depending on fragmentation amplitudes; therefore, All was distinguished from other hexoses. In MS^3 spectra generated from *m/z* 180, the relative abundance of $[M+NH_4-H_2O-NH_3]^+$ at *m/z* 163 was larger than that of $[M+NH_4-2H_2O]^+$ at *m/z* 162 for Fru, and was lower than that of $[M+NH_4-2H_2O]^+$ at *m/z* 162 for Glc (data not shown); therefore, Fru was also distinguished from other hexoses.

Distinction between MeαGlc and MeβGlc

To assess whether this technique could detect differences in the anomeric bond, MeαGlc and MeβGlc were employed. Their MS spectra showed several peaks involving $[M+H]^+$ or $[M+NH_4-NH_3]^+$ at *m/z* 195, $[M+NH_4]^+$ at *m/z* 212, $[M+Na]^+$ at *m/z* 217, $[M+NH_4-CH_4O]^+$ at *m/z* 180, and $[M+NH_4-CH_4O-NH_3]^+$ at *m/z* 163.

The MS^2 spectra generated from the precursor ion of NH_4^+ and Na^+ additives were compared under the same analytical

DOI: 10.1002/rcm

conditions. The MS^2 spectra generated from $[M+NH_4]^+$ at m/z 212 showed a larger relative abundance at m/z 180 for MeαGlc than for MeβGlc (Fig. 4(A)). The relative abundance ratios of m/z 195 to 180 or m/z 163 to 180 were significantly different between MeαGlc and MeβGlc. The relative abundance ratios of m/z 195 to 180 at the different fragmentation amplitudes are shown in Fig. 4(B).

The relative abundance ratios of m/z 195 to 180 were more than 9 at every fragmentation amplitude for MeβGlc, but were lower than 1 for MeαGlc. The two isomers could be identified by the results in Fig. 4(B). In positive ion mode, the product ions generated from $[M+Na]^+$ at m/z 217 and $[M+H]^+$ or $[M+NH_4-NH_3]^+$ at m/z 195 showed no significant differences between α and β anomers. Therefore, the two anomers (α and β) could be distinguished from MS^2 spectra using solvent supplemented with ammonium acetate to generate $[M+NH_4]^+$ ions for analysis.

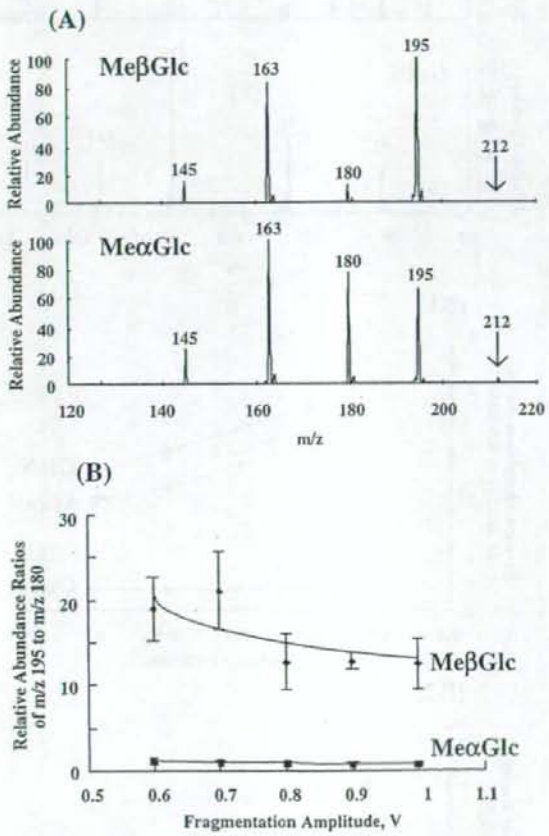

Figure 4. (A) Positive ion ESI-MS^2 spectra of MeβGlc and MeαGlc generated from precursor ion $[M+NH_4]^+$ at m/z 212. Fragmentation amplitude was 0.8 V. The precursor ion is indicated with a vertical arrow. (B) The relative abundance ratios of m/z 195 to 180 in MS^2 spectra at different fragmentation amplitudes for MeβGlc and MeαGlc. For MeαGlc, fragment ions at m/z 195 and 180 were detected above 0.6 V, for MeβGlc, the fragment ion at m/z 195 was detected above 0.5 V, and that at m/z 180 was detected above 0.6 V.

The mass spectra of isomers in negative ion mode were also investigated. In MS spectra, anions such as $[M+CH_3COO]^-$ at m/z 253 and $[M-H]^-$ at m/z 193 were detected for both anomers. In MS^2 spectra generated from precursor ions at m/z 253, a single ion species at m/z 193 was observed. Product ions such as $[M-CH_4O-H]^-$ at m/z 161, $[M-C_2H_8O_3-H]^-$ at m/z 113, and $[M-C_3H_8O_3-H]^-$ at m/z 101 were detected in MS^2 spectra generated from the precursor ion at m/z 193 in the MS spectrum. The base peak was m/z 101 for MeαGlc and m/z 161 for MeβGlc (Fig. 5(A)).

The relative abundance ratios of m/z 161 to 101 at different fragmentation amplitudes are shown in Fig. 5(B). The results showed that relative abundance ratios of m/z 161 to 101 were more than 2 at every fragmentation amplitude for MeβGlc,

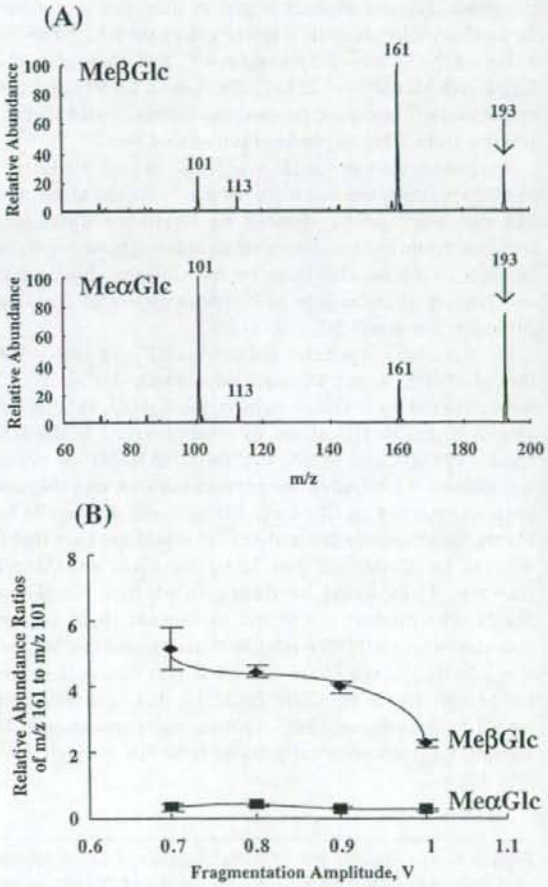

Figure 5. (A) Negative ion ESI-MS^2 spectra of MeβGlc and MeαGlc generated from precursor ion $[M-H]^-$ at m/z 193. Fragmentation amplitude was 0.9 V. The precursor ion is indicated with a vertical arrow. (B) The relative abundance ratios of m/z 161 to 101 in MS^2 spectra at different fragmentation amplitudes for MeβGlc and MeαGlc The fragment ion at m/z 101 was detected above 0.6 V, and that at m/z 161 was detected above 0.7 V for MeαGlc. The fragment ion at m/z 161 was observed above 0.6 V, and that at m/z 101 was observed above 0.7 V for MeβGlc.

DOI: 10.1002/rcm

RCM

but were lower than 0.4 for MeαGlc; the two isomers could be identified also in negative ion mode.

Therefore, MeαGlc and MeβGlc were distinguished both in positive and negative ion modes using the solvent supplemented with ammonium acetate.

Distinction between GlcN, GalN, and ManN

GlcN·HCl, GalN·HCl, and ManN·HCl in acetonitrile/water (1:1, v/v) solvent supplemented with 1 mM ammonium acetate were also examined by ESI-MS. The mass spectra showed a base peak of $[M+H]^+$ at *m/z* 180 and $[M-H_2O+H]^+$ at *m/z* 162. $[M+NH_4]^+$ at *m/z* 197 was not detected, since hexosamine with a basic NH_2 group strongly holds protons. Gas-phase basicity can be expressed in terms of gas-phase proton affinity (PA). In the gas phase, a molecule with a high gas-phase PA can abstract a proton from the protonated form of a molecule with a lower gas-phase PA.[25] The PA value of NH_3 was 204.0 kcal/mol,[26] and that of GlcN, GalN, and ManN were 223.97, 224.71, and 224.99 kcal/mol, respectively;[12] therefore, hexosamine isomers could abstract protons from NH_4^+ to produce protonated ions.

The product ion at *m/z* 162 was found in high abundance in MS^2 spectra generated from the precursor ion at *m/z* 180. MS and MS^2 spectra showed no significant differences between the three hexosamine stereoisomers; however, those isomers could be identified by the different base peaks and relative abundance in MS^3 spectra generated from the precursor ion at *m/z* 162 (Fig. 6(A)).

In the MS^3 spectra, $[M-2H_2O+H]^+$ at *m/z* 144, $[M-3H_2O+H]^+$ at *m/z* 126, and $[M-C_3H_8O_4+H]^+$ at *m/z* 72 were detected for the three isomers. $[M-C_2H_8O_4+H]^+$ at *m/z* 84 and $[C_2H_4O_2+H]^+$ at *m/z* 61 were observed in the MS^3 spectra of GlcN and ManN, and $[M-CH_8O_4+H]^+$ at *m/z* 96 was observed for GalN. The product ion that was the base peak was *m/z* 144 for GlcN, *m/z* 126 for GalN, and *m/z* 84 for ManN. Relative abundance at *m/z* 126 was larger than that at *m/z* 144 for GalN, but was lower for GlcN and ManN; therefore, GalN could be distinguished from GlcN and ManN. The product ion at *m/z* 84 showed slight relative abundance for GalN. The relative abundance of *m/z* 144 was two-fold that of *m/z* 84 for GlcN, but was almost the same for ManN; therefore, GlcN could be distinguished from ManN. Furthermore, MS^3 spectra were measured by altering fragmentation amplitudes from 0.4 through 1.0 V (Fig. 6(B)).

Since the relative abundance ratios of *m/z* 144 to 126 were 0.3–0.45 for GalN, 1–3 for ManN, and 2–5 for GlcN, GalN could be distinguished from GlcN and ManN. Moreover, GlcN and ManN were identified by relative abundance ratios

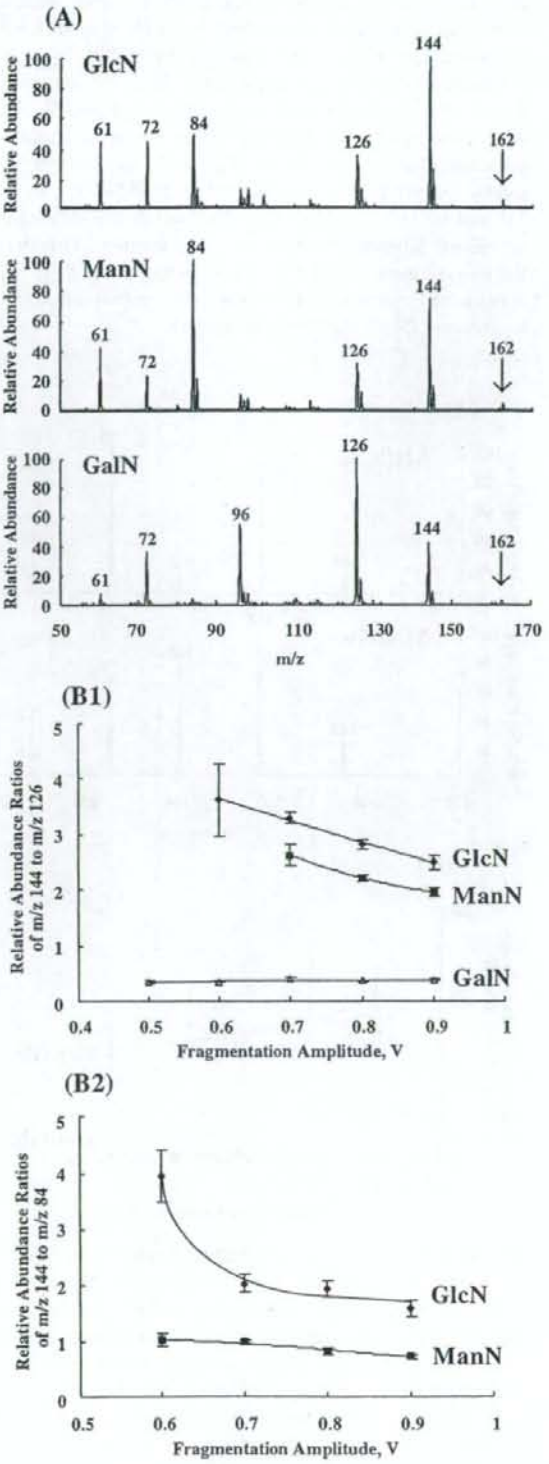

Figure 6. (A) Positive ion ESI-MS^3 spectra of GlcN, ManN, and GalN generated from precursor ion $[M-H_2O+H]^+$ at *m/z* 162. Fragmentation amplitude was 0.8 V. The precursor ion is indicated with a vertical arrow. The relative abundance ratios of (B1) *m/z* 144 to 126 and (B2) *m/z* 144 to *m/z* 84 in MS^3 spectra at different fragmentation amplitudes for GlcN, ManN, and GalN. The fragment ion at *m/z* 144 was detected above 0.5 V for GlcN and GalN, and above 0.6 V for ManN. The fragment ion at *m/z* 126 was detected above 0.5 V for GalN, 0.6 V for GlcN, and 0.7 V for ManN. The fragment ion at *m/z* 84 was detected above 0.6 V for GlcN and ManN, but not for GalN.

DOI: 10.1002/rcm